High Dynamic Range Image Generation Based on Convolutional Weight Optimization Robust to Mixed Noise Removal

Ryo Matsuoka* Shunsuke Ono† and Masahiro Okuda‡
* Kagawa University, Kagawa, Japan
E-mail: matsuoka@eng.kagawa-u.ac.jp
† Tokyo Institute of Technology, Tokyo, Japan
E-mail: ono@isl.titech.ac.jp
‡ The University of Kitakyushu, Fukuoka, Japan
E-mail: okuda-m@kitakyu-u.ac.jp

***Abstract*—Exposure blending generates a high dynamic range (HDR) image from multiple exposure images. However, when photographing in a low-light scene, these images are deteriorated due to various types of noise, and then it brings down the dynamic range. Existing methods based on pixel-wise blending cannot sufficiently reduce noise, especially in the case of a few input images. This report proposes a convolutional weight optimization method for exposure blending that robustly removes mixed noise and under/over-exposed pixels with a few inputs. In blending each pixel, the proposed method convolves neighboring pixels and generates a noise-free HDR image. The convolution of local regions enables to enhance the denoising capability of image blending. To find a set of weight maps for convolution, we introduce a weight optimization problem as a convex optimization problem, in which Huber loss function is utilized as a fidelity measure in blending to make the method robust to outliers, and solve the optimization problem by using the primal-dual splitting method. The weighted sum of the noisy input images with the estimated weight maps makes a noise-free HDR image. Experimental results show the validity of the proposed method compared with several conventional methods.**

I. Introduction

High dynamic range (HDR) imaging has ability to represent the amount of light in a scene with a broad dynamic range. Among several methods for HDR image generation, the most commonly used approach is to blend a multiple exposure image set captured by a consumer camera [1]–[11].

It is well known that the long shutter speed with a low ISO setting yields a noise-free image, however, ghosting artifacts often occur in an HDR image obtained by blending them. To avoid these artifacts, the use of a high ISO setting is efficient, because it is increasing shutter speed. Although high ISO shooting enhances noise as well as signal. Noise removal expands the dynamic range of an image, which is usually defined by the ratio between the maximum achievable signal intensity and the maximum level of camera noise.

Simply taking the mean of multiple images can help to reduce the amount of random noise with a lot of input images. However, to take dozens of images is not practice, in terms of time and storage. Several authors have recently investigated more effective exposure blending techniques based on pixel-wise weighting [1]–[8]. These methods usually generate a noise-free HDR image with less than ten images. Moreover, our previous work [12] can generate better HDR images than the other methods, especially a few inputs. However, these weighting methods cannot yield a sufficiently smooth HDR image when input images are taken with a high ISO setting in a low-light condition. This is because these methods are based on the assumption that the noise in an HDR image follows a Gaussian distribution, however, the image practically contains other types of noise, which follow some non-Gaussian distributions, and outliers. These methods do not have sufficient ability to remove them.

In this paper, we propose a convolutional exposure blending method that robustly removes mixed noise and under/over-exposed pixels by blending pixels in local regions. In our method, each pixel of a noise-free HDR image is generated by the weighted sum of local region pixels of noisy input images, and weights used in blending are determined by solving a proposed convex optimization problem. One of the features in our method is that we characterize data-fidelity by using the Huber loss function [13] that relieves influence from various outliers. Then, the convolution of local regions enables to enhance the denoising performance. An optimal solution of the proposed problem can be found via the *primal-dual splitting* (PDS) algorithm [14]. We show that the proposed method robustly removes various types of noise and saturated-pixels compared with conventional approaches.

II. Preliminaries

A. Pixel-Wise Exposure Blending

Let N be the number of pixels in an image, and $\hat{\mathbf{u}}_k \in \mathbb{R}^{3N}$, $(k = 1, 2, \cdots, K)$ be K exposure images. The conventional methods based on pixel-wise exposure blending combine the input images and reconstruct an HDR image $\mathbf{r} \in \mathbb{R}^N$ by

$$\mathbf{r} = \frac{\sum_{k=1}^{K} w_c\left(\hat{\mathbf{u}}_k\right) \otimes \tilde{\mathbf{u}}_k}{\sum_{k=1}^{K} w_c\left(\hat{\mathbf{u}}_k\right)}, \tag{1}$$

where $\tilde{\mathbf{u}}_k \in \mathbb{R}^N$ is the k-th irradiance image obtained by $\tilde{\mathbf{u}}_k := g^{-1}\left(\hat{\mathbf{u}}_k\right)/t_k$ (t_k and g^{-1} are the exposure time of the k-th image and *inverse camera response curve* function [3], respectively, which cancels the nonlinear relationship between an irradiance $\tilde{\mathbf{u}}_k$ and a camera output $\hat{\mathbf{u}}_k$). Each image is weighted by a weight function w_c. The notation $\otimes$ denotes the element-wise multiplication, and the division is also performed element by element.

In the conventional methods [1]–[3], [8], the weight function is specified to be small for the pixel values near the pixel saturation 0 and 1, high for the middle intensities, where the dynamic range of all the pixels is normalized in $[0, 1]$. An example of the weighting functions used in the conventional method [2] is given as

$$w_c(x) := \begin{cases} 2x, & \text{if } x \leq 0.5, \\ 2(1-x), & \text{if } 0.5 < x. \end{cases} \tag{2}$$

The role of the weight is to discard saturated pixels.

B. Primal Dual Splitting Algorithm

The *primal-dual splitting* (PDS) method [14] is well-known as one of the most flexible solvers for convex optimization, which finds an optimal solution of a convex optimization problem of the form:

$$\min_{\mathbf{x}} F(\mathbf{x}) + G(\mathbf{x}) + H(\mathbf{L}\mathbf{x}), \tag{3}$$

where F, G, and H are proper, lower semi-continuous, and convex functions, and F is differentiable, and $\mathbf{L}$ is a linear operator. In the PDS algorithm, the two proximity operators[1] are iteratively computed

$$\begin{cases} \mathbf{x}^{(\tau+1)} = \mathrm{prox}_{\gamma_1 G}\left(\mathbf{x}^{(\tau)} - \gamma_1\left(\nabla F\left(\mathbf{x}^{(\tau)}\right) + \mathbf{L}^{*}\mathbf{y}^{(\tau)}\right)\right), \\ \mathbf{y}^{(\tau+1)} = \mathrm{prox}_{\gamma_2 H^{*}}\left(\mathbf{y}^{(\tau)} + \gamma_2\mathbf{L}\left(2\mathbf{x}^{(\tau+1)} - \mathbf{x}^{(\tau)}\right)\right), \end{cases} \tag{4}$$

where ∇F is the gradient of F, and $\mathbf{L}^{*}$ is the adjoint of $\mathbf{L}$. The operator $\mathrm{prox}_{\gamma_2 H^{*}}$ can be computed by

$$\mathrm{prox}_{\gamma_2 H^{*}}(\mathbf{z}) := \mathbf{z} - \gamma_2 \mathrm{prox}_{H/\gamma_2}\left(\frac{\mathbf{z}}{\gamma_2}\right). \tag{5}$$

Under appropriate conditions for γ_1 and γ_2, the sequence $(\mathbf{x}^{(\bullet)})_{\bullet\in\mathbb{N}}$ weakly converges to an optimal solution of (3) (see [14] for more details).

III. Proposed Method

A. Outline

Figure 1 shows the flowchart of the proposed method. Our objective is to simultaneously perform the exposure blending and denoising. As is performed in the conventional methods [2], [3], [8], [12], we first linearize an input multiple exposure image set by Mitsunaga et al.'s method [3] to cancel the nonlinearity. Then, we obtain an initial HDR image by using the conventional blending method discussed in Sec. II-A. To achieve noise reduction, optimal weight maps are obtained by solving a convolutional weight optimization problem. Finally, we obtain a noise-free HDR image by blending input images with the estimated weight maps. Note that the proposed method performs RGB channels independently.

Our contributions are summarized as follows:

1) Convolutional exposure blending : The denoising performance of pixel-wise exposure blending is limited with a few inputs. To solve this problem, we introduce a convolutional exposure blending method. In this strategy, each blended pixel is obtained by the convolution of each local region (see Fig. 2).
2) Huber loss function : In a low-light condition, images taken with a high ISO setting are degraded by random and impulsive noise. To robust to such mixed noise, we use the Huber loss function as a fidelity term. This function involves a quadratic function near the origin and a linear function away from, it is robust to outliers (see Fig. 3).

B. Notation for Convolutional Exposure Blending

Let $\tilde{\mathbf{u}}_k \in \mathbb{R}^N$, $(k=1,2,\ldots,K)$ and $\mathbf{h} \in \mathbb{R}^N$ be linearized K exposure images and a blended image, respectively. Then, $\tilde{\mathbf{u}}_{k,i} \in \mathbb{R}^M$ be the i-th sub-vector of $\tilde{\mathbf{u}}_k$ in the i-th local region centered at i-th pixel, where M is the number of pixels in the local region. For the range of local regions, we assume a squared window or vertical/horizontal-adjacent pixels and so on. To achieve image blending, we convolve the i-th local region, for $i=1,2,\ldots,N$, by

$$r_i := \frac{\sum_{k=1}^{K}\sum_{j=1}^{M} w_{k,i,j}\tilde{u}_{k,i,j}}{\sum_{k=1}^{K}\sum_{j=1}^{M} w_{k,i,j}}, \tag{6}$$

where $\tilde{u}_{k,i,j}$ and $w_{k,i,j}$ are the j-th pixel of the sub-vector $\tilde{\mathbf{u}}_{k,i}$ and the weight map $\mathbf{w}_{k,i}$ in the i-th local region, respectively. When the weights are normalized as $\sum_k\sum_j w_{k,i,j} = 1$ for all i, it is rewritten as $r_i := \sum_k\sum_j w_{k,i,j}\tilde{u}_{k,i,j}$. To express the image blending operation in matrix form, we replicate the input images by shifting each j-th pixel of local regions to the i-th position and obtain shifted images $\mathbf{u}_l \in \mathbb{R}^N, (l=1,2,\ldots,L,$ where $L=KM)$. Then, convolutional image blending in matrix form is defined as

$$\mathbf{h} = \mathbf{U}\mathbf{w} := \sum_{l=1}^{L} \mathbf{u}_l \otimes \mathbf{w}_l, \tag{7}$$

[1] A proper lower semi-continuous convex function f over $\mathbb{R}^N$ is said to be proximable if its proximity operator for any $\gamma > 0$ can be calculated by $\mathrm{prox}_{\gamma f}(\mathbf{x}) := \arg\min_{\mathbf{y}} f(\mathbf{y}) + \frac{1}{2\gamma}\|\mathbf{x}-\mathbf{y}\|^2$.

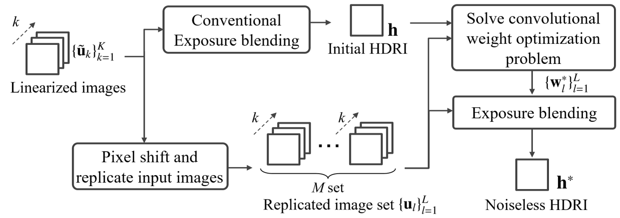

Fig. 1. Flowchart of the proposed method.

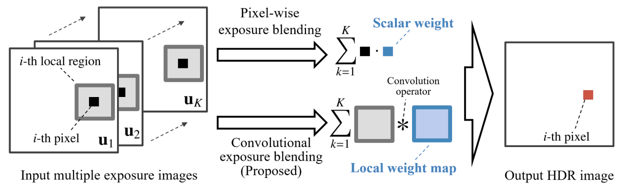

Fig. 2. Outline of Exposure Blending.

where $\mathbf{U} := [\mathrm{diag}(\mathbf{u}_1)\ \mathrm{diag}(\mathbf{u}_2)\ \ldots\ \mathrm{diag}(\mathbf{u}_L)]\ (\in \mathbb{R}^{N\times LN})$, $\mathbf{w}_l \in \mathbb{R}^N$ is the l-th weight map corresponding to $\mathbf{u}_l$, and $\mathbf{w} := [\mathbf{w}_1^\top \mathbf{w}_2^\top \ldots \mathbf{w}_L^\top]^\top (\in \mathbb{R}^{LN})$.

C. Problem Formulation

We find a set of optimal weight maps $\mathbf{w}^{*}$ such that generating a noiseless blended image $\mathbf{h}^{*}$. The proposed convolutional weight optimization problem is defined by

$$\min_{\mathbf{w}}\ \rho_{\delta,\mathbf{h}}(\mathbf{U}\mathbf{w}) + \alpha\|\mathbf{D}\mathbf{U}\mathbf{w}\|_1 \ \text{ s.t. } \mathbf{w} \in C, \sum_{l=1}^{L}\mathbf{w}_l \in \mathcal{E} \tag{8}$$

where $\mathbf{h}(\in \mathbb{R}^N)$ is a noisy HDR image obtained by the standard HDR image generation method discussed in Sec. II-A, $\mathbf{D} := [\mathbf{D}_v^\top\ \mathbf{D}_h^\top]^\top\ (\in \mathbb{R}^{2N\times N})$ is the first order differential operator, and $\mathbf{D}_v, \mathbf{D}_h \in \mathbb{R}^{N\times N}$ are the vertical and horizontal first order differential operators with Neumann boundary. The first term penalizes the similarity between a noisy HDR image $\mathbf{h}$ and a blended image obtained by the estimated weight maps $\mathbf{w}^{*}$, while the second term, which is well-known as the *total variation regularization* [15]–[18], promotes the spatial smoothness of the blended image. The parameter α is a balancing weight for the two terms. The convex sets C and $\mathcal{E}$ are defined as

$$C := \{\mathbf{x} \in \mathbb{R}^{LN} \mid x_n \in [0,1]\ \ (n = 1,2,\cdots,LN)\}, \tag{9}$$

$$\mathcal{E} := \{\mathbf{x} \in \mathbb{R}^{N} \mid |x_n - 1| \le \xi\ \ (n = 1,2,\cdots,N)\}. \tag{10}$$

By the constraints in (8), all the weights are restricted to fall within the range of $[0,1]$, and the sum of the L weights should ideally be close to 1 in order to preserve the energy after the blending operation. In this paper, a tolerable error ξ is set in consideration of calculation error.

As is discussed in Sec. III-A 2), we use the following Huber loss function [13] for the date-fidelity in the first term of (8):

$$\rho_{\delta,\mathbf{v}}(\mathbf{x}) := \sum_{n=1}^{N} H_\delta(x_n - v_n), \tag{11}$$

where

$$H_\delta(x) := \begin{cases} \dfrac{x^2}{2}, & \text{if } |x| \le \delta, \\ \delta|x| - \dfrac{\delta^2}{2}, & \text{otherwise.} \end{cases} \tag{12}$$

Since the function works as a quadratic function for small values and a linear function for large values (see Fig. 3), random and impulsive (outlier) noise can be efficiently suppressed in image blending. The

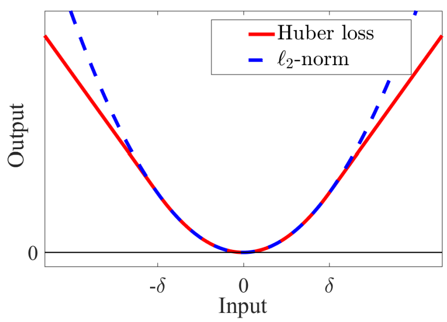

Fig. 3. Fidelity functions: The blue dashed and the red lines indicate the ℓ_2-norm and the Huber loss function, respectively, where δ determines the boundary between quadratic and linear parts.

Huber loss function is differentiable, and the gradient $\nabla\rho_{\delta,\mathbf{v}}$ is given, for $n=1,2,\ldots,N$, by [19],

$$[\nabla\rho_{\delta,\mathbf{v}}(\mathbf{x})]_n = \begin{cases} x_n - v_n, & \text{if } |x_n - v_n| \leq \delta, \\ \delta, & \text{if } x_n - v_n > \delta, \\ -\delta, & \text{if } x_n - v_n < -\delta. \end{cases} \quad (13)$$

D. Reformulation and Optimization

By using the indicator functions[2] of C and $\mathcal{E}$, the problem (8) is reformulated into an unconstrained problem

$$\min_{\mathbf{w}} \ \rho_{\delta,\mathbf{h}}(\mathbf{U}\mathbf{w}) + \alpha\|\mathbf{D}\mathbf{U}\mathbf{w}\|_1 + \iota_C(\mathbf{w}) + \iota_{\mathcal{E}}(\mathbf{E}\mathbf{w}) \quad (14)$$

where $\mathbf{E} \in \mathbb{R}^{N\times LN}$ computes the sum of the L images, which are defined as $\mathbf{E} := [\mathbf{I}_d \ \mathbf{I}_d \ \ldots \ \mathbf{I}_d]$ ($\mathbf{I}_d \in \mathbb{R}^{N\times N}$ is the identity matrix). Since the optimization problem (14) is convex, we solve it by using the PDS method described in Sec. II-B. The correspondence with each term of the objective function defined in (3) is given as follows:

$$\begin{aligned} F(\mathbf{x}) &:= \rho_{\delta,\mathbf{h}}(\mathbf{U}\mathbf{x}), \\ G(\mathbf{x}) &:= \iota_C(\mathbf{x}), \\ H(\mathbf{L}\mathbf{x}) &:= \alpha\|\mathbf{D}\mathbf{U}\mathbf{x}\|_1 + \iota_{\mathcal{E}}(\mathbf{E}\mathbf{x}), \\ \mathbf{L} &:= \begin{bmatrix} \mathbf{D}\mathbf{U} \\ \mathbf{E} \end{bmatrix} (\in \mathbb{R}^{3N\times LN}). \end{aligned}$$

From Sec. II-B, an optimal solution can be obtained by alternately calculating the following equations:

$$\left| \begin{aligned} \mathbf{w}^{(\tau+1)} &= \mathrm{prox}_{\gamma_1\iota_C}\left(\mathbf{w}^{(\tau)} - \gamma_1\left(\mathbf{U}^\top\nabla\rho_{\delta,\mathbf{h}}\left(\mathbf{U}\mathbf{w}^{(\tau)}\right) + \mathbf{L}^\top\mathbf{y}^{(\tau)}\right)\right), \\ \mathbf{y}^{(\tau+1)} &= \mathrm{prox}_{\gamma_2 H^*}\left(\mathbf{y}^{(\tau)} + \gamma_2\mathbf{L}\left(2\mathbf{w}^{(\tau+1)} - \mathbf{w}^{(\tau)}\right)\right), \end{aligned} \right. \quad (15)$$

where $\mathbf{y} := [\mathbf{y}_1^\top \ \mathbf{y}_2^\top]^\top$ ($\mathbf{y}_1 \in \mathbb{R}^{2N}$ and $\mathbf{y}_2 \in \mathbb{R}^N$). The computation of $\nabla\rho_{\delta,\mathbf{h}}$ in (15) is given by (13). The operator $\mathrm{prox}_{\gamma_2 H^*}$ in (15) is independently computed w.r.t. $\mathbf{y}_1$ and $\mathbf{y}_2$ as follows:

$$\mathbf{y}_1^{(\tau+1)} = \mathrm{prox}_{\gamma_2\|\cdot\|_1^*}\left(\mathbf{y}_1^{(\tau)} + \gamma_2\mathbf{D}\mathbf{U}\left(2\mathbf{w}^{(\tau+1)} - \mathbf{w}^{(\tau)}\right)\right), \quad (16)$$

$$\mathbf{y}_2^{(\tau+1)} = \mathrm{prox}_{\gamma_2\iota_{\mathcal{E}}^*}\left(\mathbf{y}_2^{(\tau)} + \gamma_2\mathbf{E}\left(2\mathbf{w}^{(\tau+1)} - \mathbf{w}^{(\tau)}\right)\right), \quad (17)$$

The proximity operator for the ℓ_1-norm is given by a soft-thresholding type operation as [17], [20]. The proximity operators for ι_C and $\iota_{\mathcal{E}}$ are calculated by simple clipping operations with the range of $[0, 1]$ and $[1-\xi, 1+\xi]$, respectively, as [12].

Once the optimal solution $\mathbf{w}^*$ is estimated, we obtain a noise-free HDR image by $\mathbf{h}^* = \mathbf{U}\mathbf{w}^*$.

[2]For any closed convex set $\mathcal{S}$, the indicator function is defined by $\iota_{\mathcal{S}}(\mathbf{x}) := 0$, if $\mathbf{x} \in \mathcal{S}$; ∞, otherwise.

IV. Experimental Results

To show the effectiveness of our method, we applied it to images artificially degraded by various types of noise and compared with several conventional methods. Furthermore, the proposed method is applied to real images taken with a high ISO setting.

A. Artificial Noise Removal

For quantitative evaluation, we generated "Ground truth" HDR images as follows:

(i) Input multiple exposure images: We took multiple exposure images with ISO 100, and then three images, i.e., short, middle and long exposure images, were obtained by varying the shutter speed while other camera parameters were fixed. For avoiding camera shake, we used a tripod.

(ii) Noise-free HDR image generation: The images obtained by the step (i) were simply combined by (1) with the weight function (2), yielding noise-free HDR images.

We compared our method with the two pixel-wise exposure blending methods; one is Debevec and Malik's method [2], i.e., an HDR image is obtained by (1), and the other is our previous work [12]. Moreover, our results were compared with the state-of-the-art denoising method, BM3D [21][3]. For fair comparison, we performed BM3D before and after image blending. We call the two approaches as "BM3D + MEI" and "BM3D + HDR", respectively. For the quality metric, we used the nonlinear SNR (NSNR) of generated HDR images [12]. In each method, we adjusted the degree of noise removal so as to obtain visually best restoration results, i.e., maximizing smoothness while keeping the edges of images as much as possible. In the proposed method, we used a center pixel and its adjacent four pixels (totally five pixels) as local regions, and extended image boundary by periodic expansion. The tolerable error of (10) is set to $\xi \leq 10^{-4}$.

We show the robustness of the proposed method through mixed noise removal. Mixed noise considered in this experiment includes mixed Gaussian-impulse noise and mixed Poisson-impulse noise. For the case of Gaussian noise, we set the variance to $\sigma^2 = 4.0 \cdot 10^{-3}$. For the case of Poisson noise, we generated each k-th noisy exposure image by $\hat{\mathbf{u}}'_k = \frac{1}{\lambda}D_P(\lambda\hat{\mathbf{u}}_k)$, where $\hat{\mathbf{u}}_k, \hat{\mathbf{u}}'_k$ are the k-th noise-free and noisy images, respectively, and D_P is the Poisson distribution (see [22], [23]). The scaling parameter λ was set to 0.3. We considered a salt-and-pepper noise as impulse noise and added it to the images degraded by Gaussian and Poisson noise. Note that the probability of impulse noise was set to $8.0 \cdot 10^{-4}$.

Table I shows the comparison of the NSNR for mixed Gaussian-/Poisson-impulse noise. One observes that our method achieves the best NSNR in most scenes.

In Fig. 4, some closeup of resultant HDR images are shown for mixed Gaussian- and Poisson-impulse noise, respectively. In this paper, instead of directly showing an HDR image, a low dynamic range image tone-mapped by Reinhard et al.'s local operator [24] was shown. One sees that the proposed blending method can effectively remove Gaussian/Poisson noise and impulse noise simultaneously, and yield the noise-free HDR images with preserving edges. Since employing the ℓ_2-norm for image fidelity, our previous work hardly removes impulse noise. Although those noises are almost removed by the BM3D-based methods, the details are over-smoothed, especially edges are lost in Fig. 4-(b). The proposed method based on the Huber loss function can preserve the details while removing mixed noises.

B. Real World Example

We applied the proposed method to multiple exposure images taken with a high ISO setting. Figure 5 shows all the resulting images. Note that the two scenes were taken with ISO 12800, and used for the conventional methods and our method as inputs. One sees that our method outperforms the conventional methods. From Fig. 5-(a), although the results of our previous work and "BM3D + HDR" remove strong noises, the details of bright regions are over-smoothed.

[3]We used the source code provided by the authors at http://www.cs.tut.fi/~foi/GCF-BM3D

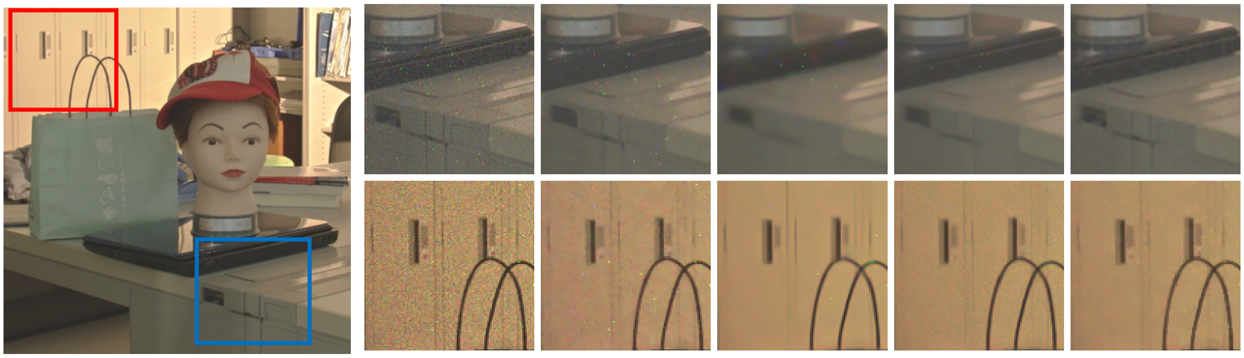

19.33 23.19 22.54 25.09 **25.72**

(a) Scene 1 in the case of Gaussian + Impulse noise

22.72 24.47 23.25 23.47 **26.68**

(b) Scene 2 in the case of Poisson + Impulse noise

Fig. 4. Closeup of some results and their NSNR: (from left to right) Debevec and Malick [2], Our previous work [12], "BM3D + HDR", "BM3D + MEI" and Our method.

TABLE I

Comparison of NSNR, Deb.: Debevec and Malick [2], Prev.: Our previous work [12], "BM3D + HDR": Applying BM3D [21] to the HDR image obtained by [2], "BM3D + MEI": the multiple exposure images denoised by BM3D and blended by [2] and Ours.

Noise	Scene	Deb.	Prev.	BM3D + HDR	BM3D + MEI	Ours
Gaussian + Impulse	1	19.33	23.19	22.54	25.09	**25.72**
	2	20.59	23.27	20.28	22.42	**24.21**
	3	19.80	24.39	23.85	25.38	**26.67**
	4	20.53	24.19	22.95	25.67	**26.45**
	5	20.79	24.72	24.97	**26.02**	25.83
Poisson + Impulse	1	21.23	24.22	24.05	25.07	**27.79**
	2	22.72	24.47	23.25	23.47	**26.68**
	3	21.81	25.36	25.08	26.59	**29.22**
	4	22.99	25.37	24.78	26.81	**28.87**
	5	22.01	25.46	25.61	25.26	**27.26**

The details of the "BM3D + MEI" were lost, while noise remains on the lower right of the upper closeup image. In addition, over-smoothing artifacts occurred in both a dark and a bright region. Our method can remove sensor noise efficiently, and preserve the image details in both dark and bright regions. Figure 5-(b) also shows that our method can remove strong noise, while preserving image details in both dark and bright regions.

From the results of both the artificial and sensor noise removal experiments, it was confirmed that the proposed blending method is more robust than the existing methods.

V. Conclusion

In this paper, we have proposed a convolutional exposure blending method for HDR image generation, in which Huber loss function is introduced as data-fidelity to robust mixed noise. In our method, convolutional weights for blending can be estimated by solving a proposed convolutional weight optimization problem that can robustly relieve various types of noise including mixed noise contamination with a few inputs. The optimization problem is solved by an efficient algorithm based on *primal-dual splitting* method. To show the validity of using the Huber loss function as data-fidelity, we applied the proposed method to noisy multiple exposure images degraded by artificial noise or sensor noise. Experimental results showed the robustness of the proposed method to various types of noise.

Acknowledgment

This work was supported by JSPS KAKENHI Grant Number JP18K18073 and MIC SCOPE(3620).

References

[1] Mann, Picard, S. Mann, and R. W. Picard, "On being 'undigital' with digital cameras: Extending dynamic range by combining differently exposed pictures," in *Proc. of IS&T*, 1995, pp. 442–448.

[2] P. E. Debevec and J. Malik, "Recovering high dynamic range radiance maps from photographs," in *ACM Trans. Graph.*, 1997, pp. 369–378.

[3] T. Mitsunaga and S. Nayar, "Radiometric self calibration," in *Proc. IEEE Conf. Comput. Vis. Pattern Recogni. (CVPR)*, vol. 1, 1999, pp. 374–380.

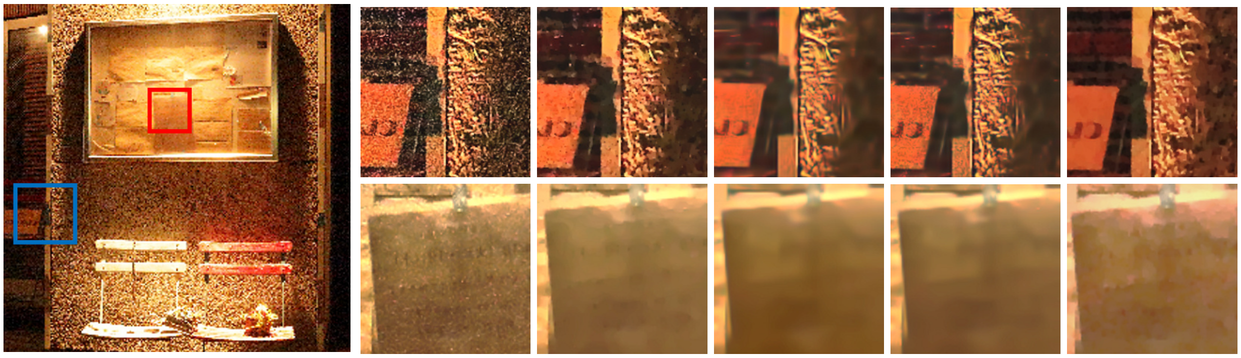

(a) Scene 6

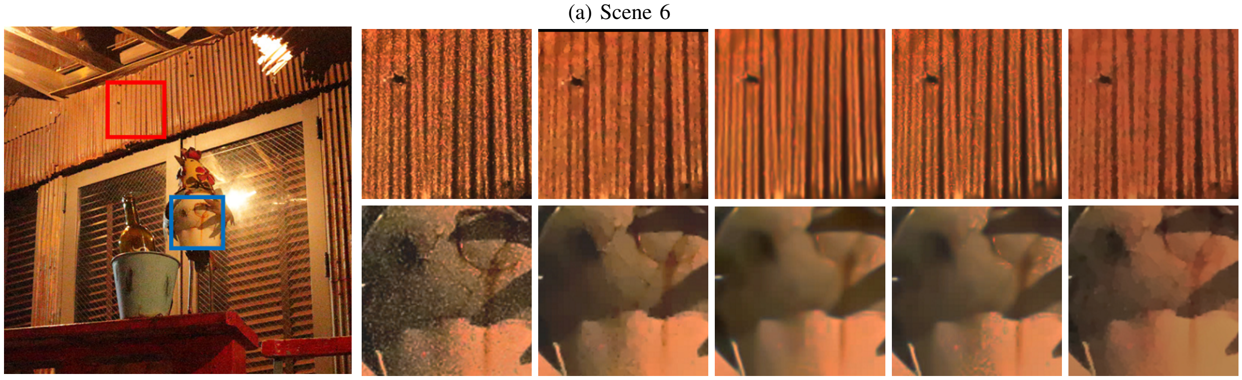

(b) Scene 7

Fig. 5. Closeup of some results in the case of sensor noise: (from left to right) Debevec and Malick [2], Our previous work [12], "BM3D + HDR", "BM3D + MEI" and Our method.

[4] E. Reinhard, G. Ward, S. Pattanaik, and P. Debevec, *High Dynamic Range Imaging: Acquisition, Display, and Image-Based Lighting (The Morgan Kaufmann Series in Computer Graphics)*. San Francisco, CA, USA: Morgan Kaufmann Publishers Inc., 2005.

[5] T. Buades, Y. Lou, J. Morel, and Z. Tang, "A note on multi-image denoising," in *Proc. Local Non-Local Approx. Image Process. Int. Workshop*, 2009, pp. 1–15.

[6] R. Matsuoka, T. Jinno, and M. Okuda, "Multiple exposure integration with image denoising," in *Proc. APSIPA Annu. Summit Conf. (APSIPA ASC)*, 2012, pp. 1–4.

[7] W. Wang and M. Ng, "A variational method for multiple-image blending," *IEEE Trans. Image Process.*, vol. 21, no. 4, pp. 1809–1822, 2012.

[8] T. Jinno and M. Okuda, "Multiple exposure fusion for high dynamic range image acquisition," *IEEE Trans. Image Process.*, vol. 21, no. 1, pp. 358–365, 2012.

[9] R. Matsuoka, T. Baba, M. Okuda, and K. Shirai, "High dynamic range image acquisition using flash image," in *Proc. IEEE Int. Conf. Acoust. Speech Signal Process. (ICASSP)*, 2013, pp. 1612–1616.

[10] R. Matsuoka, H. Ishibashi, T. Baba, and M. Okuda, "Multiple exposure integration for restoring all in-focus images," in *Proc. IEEE Int. Conf. Image Process. (ICIP)*, Sept. 2015, pp. 4165–4169.

[11] S. Hasinoff, D. Sharlet, R. Geiss, A. Adams, J. T. Barron, F. Kainz, J. Chen, and M. Levoy, "Burst photography for high dynamic range and low-light imaging on mobile cameras," *ACM Trans. Graph.*, 2016.

[12] R. Matsuoka, T. Yamauchi, T. Baba, and M. Okuda, "Weight optimization for multiple image integration and its applications," *IEICE Trans. Inf. & Syst.*, vol. E99.D, no. 1, pp. 228–235, 2016.

[13] P. J. Huber, "Robust estimation of a location parameter," *Ann. Math. Statist.*, vol. 35, no. 1, pp. 73–101, 1964.

[14] L. Condat, "A primal-dual splitting method for convex optimization involving Lipschitzian, proximable and linear composite terms," *J. Optim. Theory Appl.*, vol. 158, no. 2, pp. 460–479, 2013.

[15] A. Chambolle, "An algorithm for total variation minimization and applications," *J. Math. Imaging Vis.*, vol. 20, no. 1-2, pp. 89–97, 2004.

[16] X. Bresson and T. F. Chan, "Fast dual minimization of the vectorial total variation norm and applications to color image processing," pp. 455–484, 2008.

[17] P. L. Combettes and J.-C. Pesquet, "A proximal decomposition method for solving convex variational inverse problems," *Inverse Probl.*, vol. 24, no. 6, p. 065014, 2008.

[18] R. Matsuoka, T. Baba, M. Rizkinia, and M. Okuda, "White balancing by using multiple images via intrinsic image decomposition," *IEICE Trans. Inf. & Syst.*, vol. 98, no. 8, pp. 1562–1570, 2015.

[19] S. Ono and I. Yamada, "Signal recovery with certain involved convex data-fidelity constraints," *IEEE Trans. Signal Process.*, vol. 63, no. 22, pp. 6149–6163, 2015.

[20] S. Ono and I. Yamada, "Color-line regularization for color artifact removal," *IEEE Trans. Comput. Imaging*, vol. 2, no. 3, pp. 204–217, 2016.

[21] K. Dabov, A. Foi, V. Katkovnik, and K. Egiazarian, "Image denoising by sparse 3-d transform-domain collaborative filtering," *IEEE Trans. Image Process.*, vol. 16, no. 8, pp. 2080–2095, 2007.

[22] R. Puetter, T. Gosnell, and A. Yahil, "Digital image reconstruction: Deblurring and denoising," *Annu. Rev. Astron. Astrophys.*, vol. 43, no. 1, pp. 139–194, 2005.

[23] S. Ono and I. Yamada, "Poisson image restoration with likelihood constraint via hybrid steepest descent method," in *Proc. IEEE Int. Conf. Acoust. Speech Signal Process. (ICASSP)*, 2013, pp. 5929–5933.

[24] E. Reinhard, M. Stark, P. Shirley, and J. Ferwerda, "Photographic tone reproduction for digital images," *ACM Trans. Graph.*, vol. 21, no. 3, pp. 267–276, 2002.